

Optimal Time-Domain Detection of a Deterministic Target Buried Under a Randomly Rough Interface

Traian Dogaru, Leslie Collins, *Member, IEEE*, and Lawrence Carin, *Senior Member, IEEE*

Abstract—We consider pulsed plane-wave scattering from targets buried under a rough air–ground interface. The properties of the interface are parametrized as a random process with known statistics, and therefore the fields scattered from a particular surface constitute one realization of an ensemble, characterized by corresponding statistics. Moreover, since the fields incident upon a buried target must first penetrate the rough interface, they and the subsequent scattered fields are random processes as well. Based on this understanding, an optimal detector is formulated, accounting for the clutter and target-signature statistics (the former due to scattering at the rough surface, and the latter due to transmission); the statistics of these two processes are in general different. Detector performance is compared to that of a matched filter, which assumes the target signature is known exactly (i.e., nonrandom). The results presented here, as a function of angle and polarization, demonstrate that there is often a significant gain in detector performance if the target signature is properly treated as a random process.

Index Terms—Optimal detection, rough surface scattering, time-domain analysis.

I. INTRODUCTION

THE scattering of waves at a rough surface has motivated considerable research [1]–[9]. These studies have been performed primarily in the frequency domain, although there have been some recent time-domain investigations [7], [9]. The rough surface is usually parametrized as a random process (i.e., while the details of a particular realization of the surface are not known exactly, each surface is assumed to represent one realization of an ensemble, characterized by known statistics). Since the rough surface is treated statistically, the fields scattered and transmitted (for penetrable surfaces) at such a surface must be parametrized statistically as well. In the frequency domain, the fields scattered at a given frequency are parametrized as a random variable [1]–[8], usually by the mean and variance (under the assumption that the random variable has a Gaussian distribution). For time-domain scattering, the fields must be parametrized as a random process [9]. In our previous investigation of transient scattering from a Gaussian rough surface [9], we have found the backscattered fields to be wide-sense-stationary and Gaussian; however, the data was correlated (i.e., it was *not-white*).

Manuscript received October 27, 1997; revised April 19, 2000. This work was supported in part by the Army Research Office under Grant DAAH04-96-1-0448 (Demining MURI), the Army Research Laboratory (Adelphi, MD), and by the Office of Naval Research under Grant N00014-96-1-0861.

The authors are with the Department of Electrical and Computer Engineering, Duke University, Durham, NC 27708-0291 USA.

Publisher Item Identifier S 0018-926X(01)01270-4.

The statistics of fields scattered by a rough surface are of interest for many applications. For example, such statistics can be used to infer properties of the rough surface, of interest for remote sensing of soil or vegetation [4]–[6]. In the work presented here, we are interested in detection of a target situated near a rough surface, for which the rough-surface-induced scattered fields are usually characterized as clutter. In detection applications, the clutter statistics are often used to prewhiten the data [9]–[11], representing the initial stage in most detectors.

The most commonly used scheme for detection of transient signals is the matched filter [10], in which the target signature is assumed known exactly. However, as discussed above, the fields transmitted through a penetrable rough surface constitute a random process (like the surface-scattered fields), and therefore the fields that impinge upon a buried target are, in turn, random (further randomness can incur if the medium under the surface is itself random [6], although this is not considered here). Therefore, even if the buried target is known exactly (but the rough surface is treated statistically), its scattered fields must be treated as a random process. In a previous paper [9], we have demonstrated that, in many cases, the random quality of the target signature results in matched-filter detector performance—quantified in terms of probability of detection versus probability of false alarm, termed the receiver operating characteristic (ROC)—which is significantly inferior to the expectations of ideal matched-filter theory (which assumes all underlying assumptions are valid). In this paper, we consider implementation of an optimal detector which properly accounts for the random nature of the target's scattered signature.

The development of an optimal detector for a random signal in noise (clutter) requires *a priori* knowledge of both the target and clutter statistics. As discussed above, a whitening filter is generally used to convert the clutter into a white process. The whitening filter is implemented using the clutter correlation matrix [10], [11], computed here via Monte Carlo simulations for scattering from the rough surface alone, in the absence of buried targets (as would be done for the experimental collection of clutter statistics). Therefore, while frequency-domain fields scattered from a rough surface are parametrized by their mean and variance, here time-domain scattering (a random process) is characterized via its correlation matrix. Having quantified the statistics of time-domain rough-surface scattering, it remains to account for the statistics of the stochastic buried-target signature.

As discussed subsequently, an optimal scheme for detection of a random signature requires integration over the signature's density function [10]. Unfortunately, such a density function is difficult to obtain in general. Therefore, we implement the

optimal detector approximately via Monte Carlo integration, through consideration of multiple realizations of the target signature (each for a particular rough surface, from an ensemble of such). Thus, instead of requiring the statistics of the target response, *per se*, we only require access to a set of target signatures representative of such. Multiple waveforms are calculated here using a forward-scattering algorithm. Recall from above that, in principle, clutter statistics can be measured and therefore a forward algorithm is not essential for such. However, to build an optimal detector, one requires multiple realizations of the target signature, for different manifestations of the rough surface. A fast forward-scattering algorithm is therefore essential for optimal detection of such targets, with random scattering signatures (the statistics of which are not easily measured for variable targets and target positions). While fast algorithms are well known to be requisite elements in inverse-scattering schemes (generally for deterministic scattering data) [12], [13], here we introduce the use of such in optimal detectors (for stochastic scattering data).

The optimal detector is of general utility, with results presented here for the special case of two-dimensional scattering. All scattering data are computed via a finite-difference time-domain (FDTD) algorithm [14]–[30], in which we consider plane-wave incidence and far-zone scattering, using an appropriate near-to-far-zone transformation [9], [30]. Moreover, since this algorithm must be run many times—to compute clutter statistics, multiple realizations of the stochastic target signature, as well as for generation of ROC curves—it is essential that the FDTD be as fast as possible. To reduce the computational domain, we have utilized the perfectly-matched-layer (PML) absorbing-boundary condition [23]–[25], with appropriate modifications for handling lossy soil [26], [27].

The remainder of the paper is organized as follows. In Section II we develop the optimal detector for targets with random scattering signatures. Since the fast forward-scattering algorithm is an integral element of such, it is discussed in this section. Results are presented in Section III, for both TE and TM polarization, wherein comparisons are performed with the idealized matched filter. Conclusions are discussed in Section IV, as are directions for future research.

II. OPTIMAL DETECTOR

A. Target-Signature Model

We consider development of an optimal detector for known targets buried under a rough interface. In a previous paper [9], we investigated the matched filter and evaluated its performance. The matched filter is optimal if the target signature is known exactly and the noise (clutter) is Gaussian and wide-sense stationary. In our previous work [9], we have found that a Gaussian rough surface yields clutter which is Gaussian and wide-sense stationary, although it has been found to be correlated. Therefore, for the problem considered here, the matched filter is preceded by a whitening filter [10].

Having verified that the *clutter* meets the requirements of a matched filter, it remains to investigate the characteristics of the target signature. The assumption of a deterministic target re-

sponse is investigated by comparing the receiver operating characteristics (ROCs) obtained via Monte Carlo simulation with *idealized* ROC curves, computed presupposing that all underlying assumptions are valid. In such computations, a natural choice for the “known” target signature is its response when buried under a flat interface, represented in discretized form by the N -dimensional vector $\mathbf{s} = [s_1 \ s_2 \ \dots \ s_N]^T$; the discretized measured field and clutter are similarly expressed as $\mathbf{e} = [e_1 \ e_2 \ \dots \ e_N]^T$ and $\mathbf{c} = [c_1 \ c_2 \ \dots \ c_N]^T$, respectively. Therefore, the matched filter assumes that under hypothesis H_1 (target plus clutter) $\mathbf{e} = \mathbf{s} + \mathbf{c}$, while under hypothesis H_0 (clutter only) $\mathbf{e} = \mathbf{c}$. In light of the fact that the clutter as measured is not white, we assume \mathbf{e} , \mathbf{s} , and \mathbf{c} have been passed through a whitening filter. In the Bayesian approach [10], we partition the observation space into two regions, corresponding to the two hypotheses, such that the cost of the decision is minimized. This is done by transforming the N -dimensional problem into a one-dimensional likelihood ratio test

$$\Lambda(\mathbf{e}) = \frac{p_c(\mathbf{e} - \mathbf{s})}{p_c(\mathbf{e})} \quad (1)$$

where $p_c(\cdot)$ is the probability distribution function of the clutter \mathbf{c} . The likelihood ratio is compared against a threshold T [10], and we decide that the signal is present if $\Lambda(\mathbf{e}) > T$ and it is not present if $\Lambda(\mathbf{e}) < T$. After prewhitening the Gaussian clutter, the natural log of (1) yields the conventional matched-filter sufficient statistic [10] $l = \mathbf{e}^T \mathbf{s}$.

The ROCs give a measure of the detector performance, through consideration of the probability of detection (P_D) versus the probability of false alarm (P_F). By definition,

$$\begin{aligned} P_D &= \int_T^\infty p(\Lambda|H_1) d\Lambda \\ P_F &= \int_T^\infty p(\Lambda|H_0) d\Lambda \end{aligned} \quad (2)$$

where $p(\Lambda|H_i)$ is the probability of Λ for hypothesis H_i . It can be shown that, for the case of additive white Gaussian noise (after prewhitening), the probabilities of detection and false alarm depend only on the parameter $d = E/\sigma^2$, where E is the energy of the target response and σ^2 is the noise variance [10].

Therefore, from E and σ^2 , one can readily compute the *theoretical* ROC, representative of idealized detector performance, if all the assumptions mentioned earlier are valid. By comparing these theoretical characteristics with the ones obtained by Monte Carlo simulation (considering a large number of surface realizations), we have determined in [9] that the actual detector performance is often well below that of the ideal, especially for near-grazing incidence. We attributed this to an inappropriateness of the deterministic-target-response assumption.

B. Optimal Detector

One can model the randomness in the target response by introducing a generalized stochastic parameter $\boldsymbol{\theta}$. Instead of assuming the target signature \mathbf{s} is known exactly, we introduce an uncertainty which we symbolize by introducing the notation $\mathbf{s}(\boldsymbol{\theta})$, where $\boldsymbol{\theta}$ represents a vector of stochastic parameters that

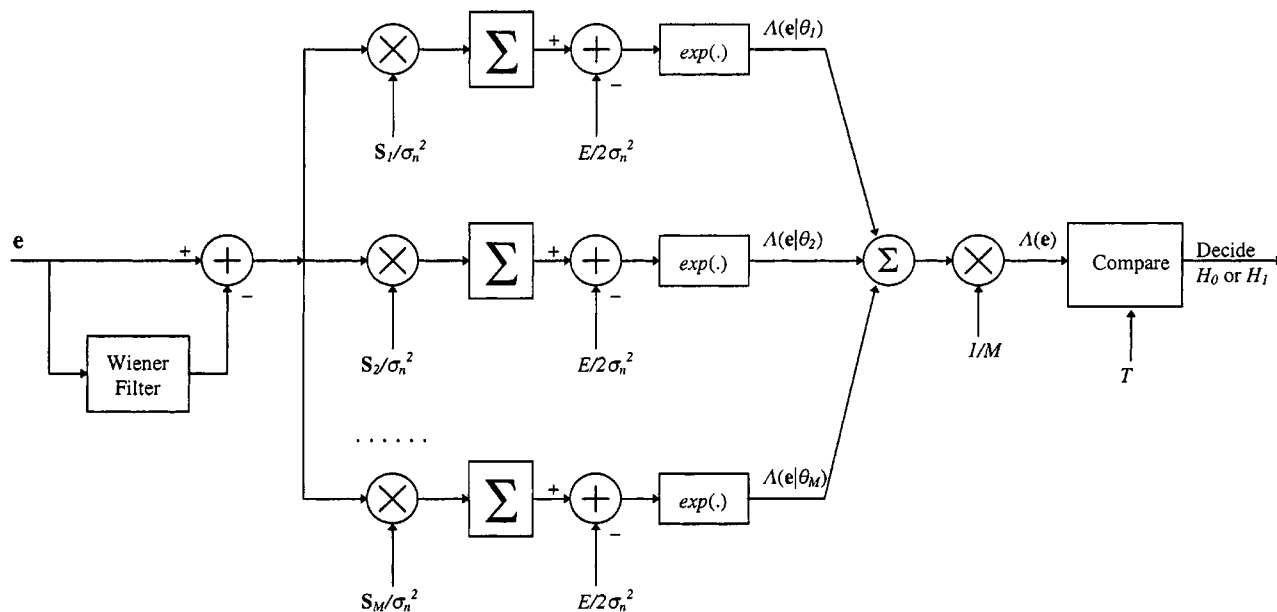


Fig. 1. Optimal detector for a random signal in additive clutter, using a Wiener whitening filter and M realizations of the random signature.

are responsible for the random nature of \mathbf{s} . Thus, under the hypothesis H_1 , the received signal becomes $\mathbf{e} = \mathbf{s}(\boldsymbol{\theta}) + \mathbf{c}$. The previous, simple likelihood ratio is now generalized as

$$\Lambda(\mathbf{e}) = \frac{\int p_c[\mathbf{e} - \mathbf{s}(\boldsymbol{\theta})] p_{\boldsymbol{\theta}}(\boldsymbol{\theta}) d\boldsymbol{\theta}}{p_c(\mathbf{e})} = \int \Lambda(\mathbf{e}|\boldsymbol{\theta}) p_{\boldsymbol{\theta}}(\boldsymbol{\theta}) d\boldsymbol{\theta} \quad (3)$$

where $\Lambda(\mathbf{e}|\boldsymbol{\theta})$ represents the likelihood ratio for a particular $\mathbf{s}(\boldsymbol{\theta})$ and $p_{\boldsymbol{\theta}}(\boldsymbol{\theta})$ is the probability density function of the vector $\boldsymbol{\theta}$.

Note that we have not specified $\boldsymbol{\theta}$, nor do we quantify its distribution. Even though there are ways to model $\boldsymbol{\theta}$ as a physical quantity, we avoid this and consider an alternative manner of computing the likelihood ratio. Considering (3), note that the expression on the right side is simply the ensemble average of $\Lambda(\mathbf{e}|\boldsymbol{\theta})$, computed for all possible values of $\boldsymbol{\theta}$. We can approximate this quantity numerically by performing Monte Carlo integration. Thus, we consider M realizations of the random vector $\boldsymbol{\theta}$, the m th of which is represented by $\boldsymbol{\theta}_m$ (physically corresponding to M realizations of the rough surface), and compute the approximate likelihood ratio as

$$\Lambda(\mathbf{e}) = \int \Lambda(\mathbf{e}|\boldsymbol{\theta}) p_{\boldsymbol{\theta}}(\boldsymbol{\theta}) d\boldsymbol{\theta} \approx \frac{1}{M} \sum_{m=1}^M \Lambda(\mathbf{e}|\boldsymbol{\theta}_m). \quad (4)$$

Consequently, we obtain the structure of the optimal receiver described in Fig. 1.

The whitening filter is implemented as a forward linear prediction-error filter [31]. A linear prediction filter is a Wiener filter, with tap weights represented by the vector $\mathbf{w} = [w_0, w_1 \dots w_P]^T$, (P th-order filter) satisfying the Yule-Walker equation $\mathbf{R}\mathbf{w} = \mathbf{r}$, where $r_k = E[c_n c_{n+k}]$, $\mathbf{r} = [r_1 \ r_2 \ \dots \ r_P]^T$, and \mathbf{R} represents the correlation matrix $E[\mathbf{c}\mathbf{c}^T]$, which, for a wide-sense stationary process, has Toeplitz symmetry.

C. Numerical Model

The data used in our study are obtained by numerical simulation using a two-dimensional finite-difference time-domain code (with no variation in the z direction, see Fig. 2). We use the standard Yee cell [14], for both TE and TM polarization. Plane-wave excitation is considered, employing a (total field)–(scattered field) formulation [9], [19], [20]. The backscattered fields to be processed are observed in the far zone, necessitating a near-to-far zone transformation [9], [30], with separate Huygens surfaces used to enclose the target and the rough surface (Fig. 2). Finally, with regard to the rough air–ground interface, it has been demonstrated that the staircase approximation to such (inherent to the Yee scheme) is accurate, as long as the grid size is very small compared with the wavelength, the surface correlation length, and the surface variance [7].

To implement the detector, we must first characterize $p_c(\mathbf{e})$, which requires hundreds of rough-surface realizations (N_c), in the absence of a target. Subsequent implementation of the detector in (4), for a given \mathbf{e} , requires computation of the likelihood ratios $\Lambda(\mathbf{e}|\boldsymbol{\theta}_m)$, therefore requiring M realizations of $\mathbf{s}(\boldsymbol{\theta}_m)$; in the subsequent examples, we demonstrate that, for the data considered here, M must be on the order of forty. Finally, \mathbf{e} is a random process (and therefore $\Lambda(\mathbf{e}|\boldsymbol{\theta}_m)$ a random variable). Therefore, the *statistical* detector characterization requires consideration of N_e realizations of the scattered signal \mathbf{e} , where here we have considered N_e on the order of several hundred. Therefore, detector implementation and characterization requires $2M + N_e + N_c$ scattered-field computations (the factor two in $2M$ is clarified below). Therefore, it is critical that the modeling algorithm be as computationally efficient as possible.

To achieve computational efficiency, it is essential that the FDTD computational domain be as small as possible. Therefore, we have employed a PML absorbing medium for the outwardly

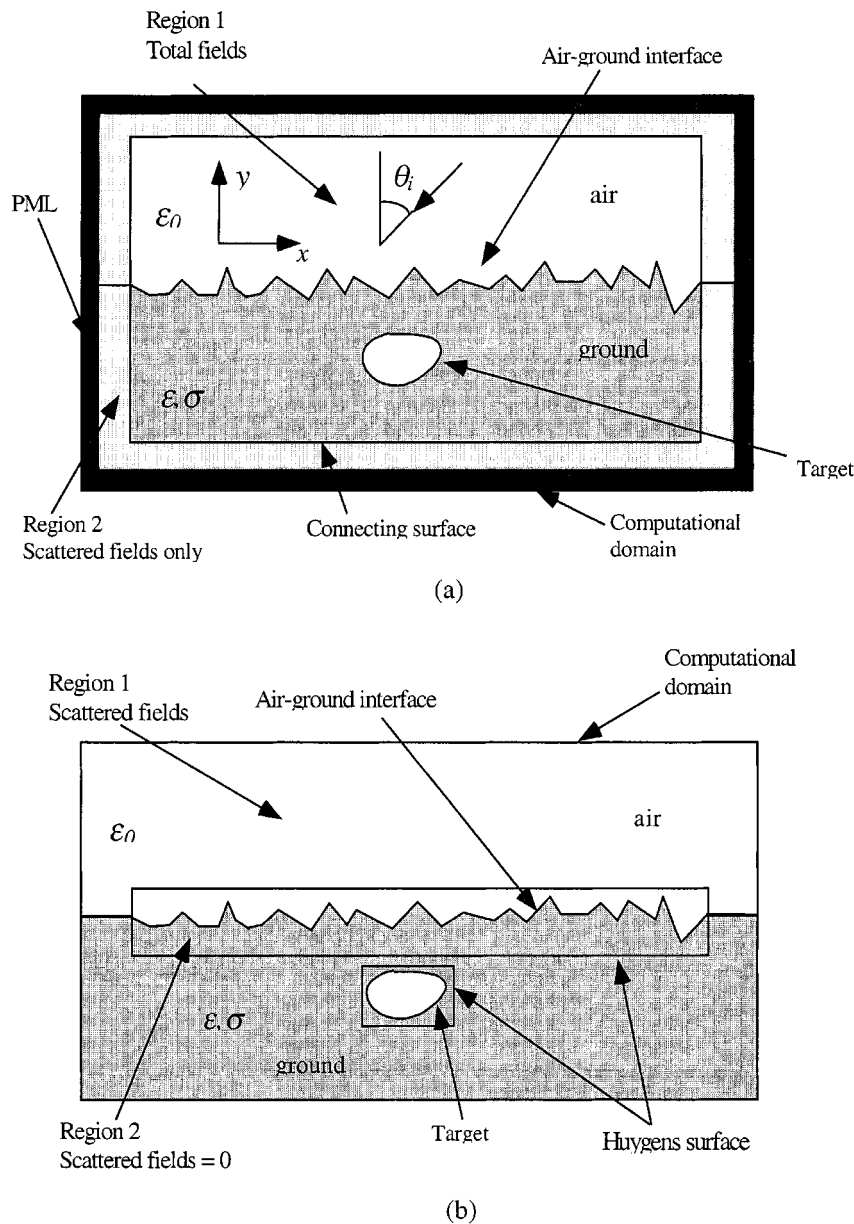


Fig. 2. Schematization of the buried-target problem and the finite-difference time-domain algorithm used for its modeling. (a) Target buried under a rough surface. (b) Summary of FDTD algorithm.

propagating waves leaving the computational domain. The PML used here is designed to absorb waves in lossy media [26], [27], of interest for the lossy half space. For the problems studied, we have employed the incident pulse shown in Fig. 3, representative of a Rayleigh wavelet [32], and have utilized 12 FDTD spatial samples per wavelength, for the smallest wavelength of interest in the problem. The computational size of each FDTD calculation was $9\lambda_c \times 1.5\lambda_c$ (width \times depth), where λ_c is the center wavelength of the incident pulse (Fig. 3) in free space. For this problem size and spatial discretization numerical dispersion [17], [18] was not found to present a problem.

Before proceeding to the results, we reiterate that we have considered plane-wave incidence, motivated by ground-penetrating systems with a large stand-off distance. For example, ultrawideband synthetic aperture radar (SAR) systems [33], [34] employ sensors that are quite distant from the target, for which

plane-wave incidence appears most appropriate. However, this introduces a problem. In particular, diffraction is induced at the ends of the numerical rough surface (see Fig. 2), with such *not* representative of the statistics of the rough surface itself. To mitigate this problem, several authors have considered beam excitation [1], [2], [7], which removes the edge effects but also solves a problem different from the plane-wave case of interest. For beam excitation, one could make the beamwidth large enough such that, at least paraxially, a reasonable plane-wave approximation could be made; however, this results in a significant increase in the computational domain. Moreover, we note that previous beam-excitation studies (e.g., [1], [2], [7]) have considered narrow-band problems, while here we are addressing ultrawideband fields (see Fig. 3). For such, one has the added complexity of requiring the beamwidth to be wide relative to *all* wavelengths in the incident pulse, which would require pro-

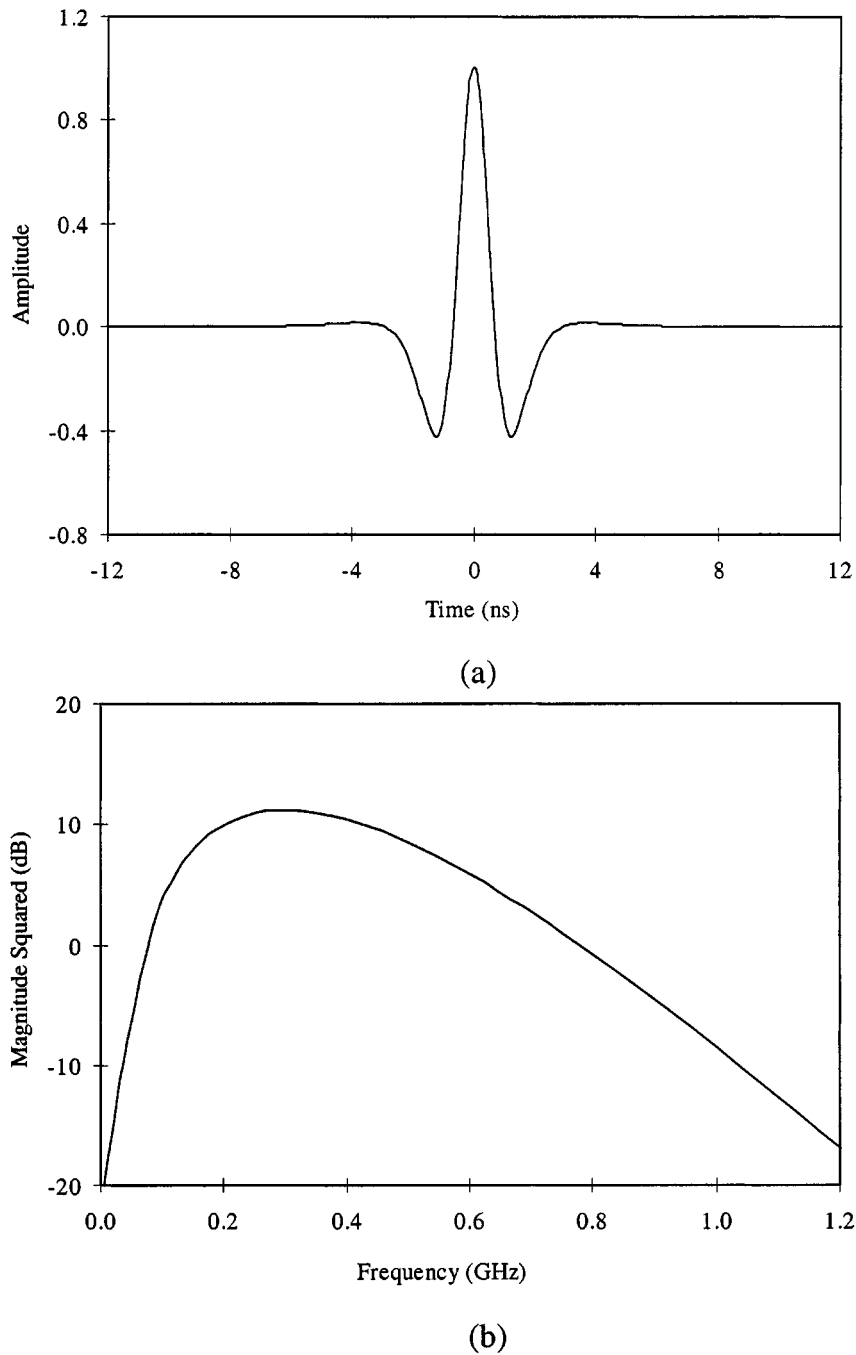


Fig. 3. Incident pulse and corresponding spectrum used in the numerical computations. The energy is peaked at a center frequency of 300 MHz ($\lambda_c = 1$ m). (a) Time-domain waveform. (b) Spectrum.

hibitively wide beams (and hence very large computational domains) at the low frequencies of interest in the pulses used for ground-penetration applications.

Fortunately, for the detector problem of interest here, these difficulties are avoided to a large extent. In particular, for the white Gaussian clutter (after prewhitening) \mathbf{c} , the optimal detector in (4) reduces to projecting the measured signal \mathbf{e} onto M realizations of $\mathbf{s}(\boldsymbol{\theta}_m)$. For the targets considered here, $\mathbf{s}(\boldsymbol{\theta}_m)$ is nonzero over a relatively limited temporal support, and it is only over this time that the values of \mathbf{e} are important to detector performance. For the geometrical parameters considered here, the edge-diffraction-induced effects in \mathbf{e} are well outside the tem-

poral support of $\mathbf{s}(\boldsymbol{\theta}_m)$, and therefore have no impact on detector performance. We also note that, for the same reasons, the only portion of the clutter \mathbf{c} meaningful to detector performance is that in the vicinity of the nonzero support of $\mathbf{s}(\boldsymbol{\theta}_m)$; therefore, it was also this portion of \mathbf{c} that was used to compute the clutter correlation matrix \mathbf{R} .

Although the above discussion addresses concerns of edge diffractions induced at the end of the numerical rough surface, we have not accounted for the fact that such diffractions may launch surface waves that would not be present in an actual rough surface (without such endpoints). We have carefully examined the backscattered clutter \mathbf{c} , to see if such surface waves

are induced (as witnessed in [1] for a highly conducting interface). Such effects, if present, were within the noise of the numerical results and were therefore deemed unimportant for the relatively low-loss medium considered here. Therefore, while plane-wave incidence presents unavoidable problems at the ends of the numerical rough surface, for the ultrawideband applications of interest, beam excitation is not a viable alternative; moreover, for the reasons discussed above, plane-wave excitation does not appear to produce significant problems for the detection problems and material properties considered here.

III. RESULTS

In the examples considered here, we assume a Gaussian rough surface, with zero mean, standard deviation 3.95 cm, and correlation length 18.75 cm. This distribution is felt reasonable for many air–soil interfaces, but it is *not* based on the measured properties from any particular interface. Other parameters and distributions are clearly possible (and, possibly, in some cases more realistic). However, Gaussian interfaces have been well studied [1]–[9] and constitute a good starting point. The soil is represented by a lossy dielectric with $\epsilon_r = 6$ and conductivity $\sigma = 0.005\text{S/m}$, which is characteristic of many soil types [35]. Finally, the target is placed 25 cm under the mean air–ground interface position, and consists of a lossless dielectric with $\epsilon_r = 2$, a width of 37.5 cm (“parallel” to the interface), and a thickness of 12.5 cm. We consider both TE and TM polarizations and plane-wave incidence at 30° and 70° , with respect to the normal (see Fig. 2). Finally, in all cases the incident pulse shape corresponds to the Rayleigh wavelet in Fig. 3, with bandwidth representative of current ground penetrating radar systems.

A. Signature of Target Buried Under a Flat Interface

As discussed in Section II-A, the matched-filter detector is effected by projecting the measured data \mathbf{e} onto a canonical waveform, here the response of the target when buried under a flat surface, thereby yielding the test statistics $l = \mathbf{e}^T \mathbf{s}$ (\mathbf{s} is the target response for a *flat* interface). It is therefore of interest to examine the characteristics of \mathbf{s} , as well as the statistics of the clutter \mathbf{c} , which are fundamental to detector performance.

The properties of \mathbf{s} are addressed in Fig. 4(a) and (b), in which the energy spectral density (ESD) of \mathbf{s} is investigated for TE and TM excitation, considering angles of incidence $\theta_i = 30^\circ$ and $\theta_i = 70^\circ$, respectively. For the soil considered here, the Brewster angle is 67.8° (neglecting the effects of the conductivity σ). We see that, over much of the spectrum, for $\theta_i = 70^\circ$ the far-zone backscattered fields are stronger for TM excitation than for TE, consistent with the enhanced penetration expected for TM polarization near the Brewster angle. For incidence angle $\theta_i = 30^\circ$ (well away from the Brewster angle), the energy spectral densities for TE and TM excitation are very similar. We note that the polarization and incidence-angle dependence of the target itself, apart from the Brewster-angle effects at the interface, also play a significant role concerning the results in Fig. 4.

B. Clutter Statistics

From Fig. 4, one might expect that, for near-Brewster incidence, a matched filter would perform better for TM polariza-

tion than for TE, assuming the underlying matched-filter assumptions are valid: that the target signature is deterministic and similar to that for a target under a flat interface. However, detector performance is strongly influenced by the clutter characteristics, the power spectral density (PSD) for which are shown in Fig. 5, using the surface statistics, polarizations, and incidence angles considered above. We see from Fig. 5 that the PSD is stronger for TM excitation than for TE, appreciably so for $\theta_i = 70^\circ$. Therefore, it is possible that detector performance will actually be worse for near-Brewster TM excitation, as compared to TE incidence at the same angle, despite the fact that the flat-surface target response is larger for TM incidence. Note that the clutter is nonwhite (is correlated), and the detector performance will ultimately be determined by the properties of the whitened clutter. Nevertheless, the results in Figs. 4 and 5 indicate that the assumption of optimal detector performance for near-Brewster TM excitation may be undermined by the properties of the rough-surface-generated clutter.

C. Detector Performance

In the next series of figures, we demonstrate ROC performance for the detectors discussed in Section II, considering the geometrical properties and operating conditions addressed in Figs. 4 and 5. In each figure, three results are presented: idealized matched-filter performance, assuming all underlying assumptions are valid; actual matched filter performance; and detector performance for the optimal detector in (4), using $M = 50$ (for the examples considered here, the results stabilized for $M > 40$). The idealized matched-filter results were computed by applying the matched filter to $N_e = 300$ *synthesized* waveforms, constructed by adding the flat-surface target response to 300 realizations of the fields scattered from the rough surface, in the absence of a buried target (these were *not* the same $N_e = 300$ clutter realizations used to design the whitening filter). Actual matched-filter performance was computed using $N_e = 300$ realizations of fields scattered from a target buried under a randomly rough surface (making no assumptions that the target signature is deterministic). This same scattering data was used to characterize the optimal detector in (4).

To effect the optimal detector, we require M realizations of the target signature $\mathbf{s}(\boldsymbol{\theta}_m)$, which must characterize the statistical variation of $\mathbf{s}(\boldsymbol{\theta})$, dictated by $p_{\boldsymbol{\theta}}(\boldsymbol{\theta})$. To compute $\mathbf{s}(\boldsymbol{\theta}_m)$, we consider M realizations of the rough surface, and for each we run the FDTD code twice: once with the target and once without, obtaining $\mathbf{c}_m + \mathbf{s}(\boldsymbol{\theta}_m)$ and \mathbf{c}_m , respectively. The difference between these two waveforms is defined to be $\mathbf{s}(\boldsymbol{\theta}_m)$, for use in (4). Thus, we parametrize the target signature as random and explicitly enforce (by definition) the additivity of the target signature and clutter, both of which are random.

In Figs. 6 and 7, we plot ROC curves for TE and TM polarization, respectively, for incidence angle $\theta_i = 30^\circ$. From Figs. 4(a) and 5(a), for $\theta_i = 30^\circ$, the target ESD and clutter PSD are very similar for TE and TM polarization. In fact, defining E_{TE} and E_{TM} as the energies in the flat-surface target signatures for TE and TM polarization, respectively, we have found that $E_{\text{TM}}/E_{\text{TE}} = 1.416$ for $\theta_i = 30^\circ$. Moreover, defining σ_{TE}^2 and σ_{TM}^2 as the clutter variance for TE and TM polarization, respectively, we have found that, for $\theta_i = 30^\circ$, $\sigma_{\text{TM}}^2/\sigma_{\text{TE}}^2 = 1.584$.

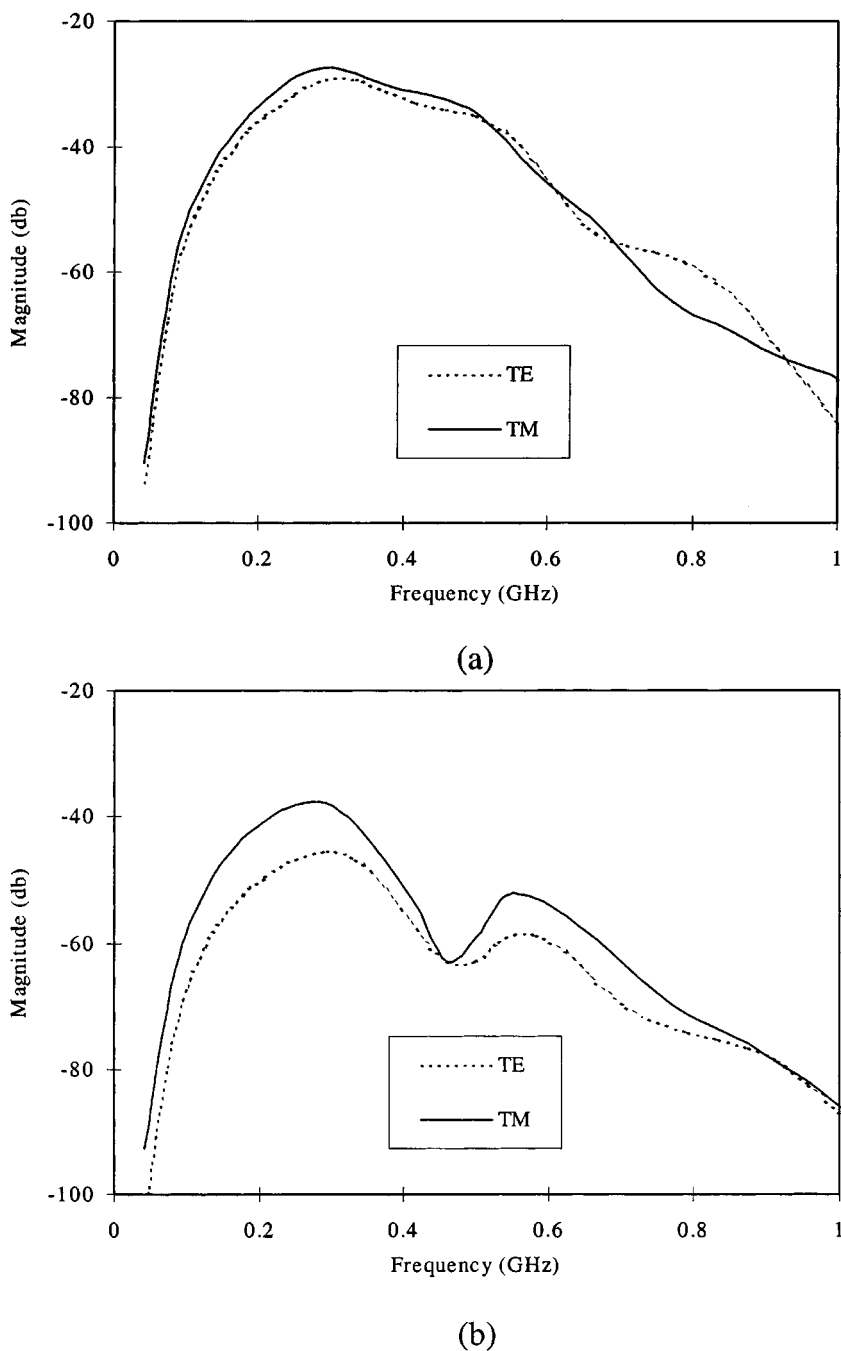


Fig. 4. Energy spectral density of a 37.5 cm \times 12.5 cm dielectric target ($\epsilon_r = 2$) buried 25 cm beneath a flat air–ground interface, with the lossy soil characterized by $\epsilon_r = 6$ and $\sigma = 0.005$ S/m. Results are plotted for both TE (horizontal) and TM (vertical) polarization. (a) Incidence angle $\theta_i = 30^\circ$. (b) Incidence angle $\theta_i = 70^\circ$.

The similarity of the target energies and clutter variances for TE and TM polarization forecasts the similarity in detector performance manifested in Figs. 6 and 7, for $\theta_i = 30^\circ$. The other significant observation from these figures. is that, for $\theta_i = 30^\circ$, the optimal detector performs only slightly better than the simple matched filter. This issue will be addressed after first examining performance for incidence angle $\theta_i = 70^\circ$.

In Figs. 8 and 9 we consider detector performance for TE and TM polarizations, respectively, for an incidence angle of $\theta_i = 70^\circ$. For this example, using the same notation as above, $E_{TM}/E_{TE} = 5.671$ and $\sigma_{TM}^2/\sigma_{TE}^2 = 11.018$. Therefore,

it is not surprising that, for $\theta_i = 70^\circ$, the detectors perform markedly better for TE polarization than for TM (reduced false alarms required to achieve a given detection probability), despite the fact that the angle of incidence is very near the Brewster angle. While the ratios E_{TM}/E_{TE} and $\sigma_{TM}^2/\sigma_{TE}^2$ predict that the detector will perform better for TE polarization than for TM, they do not explain the other principal feature of these results: for TE polarization, the actual matched-filter performance is significantly degraded relative to idealized results, and the optimal detector yields a significant performance enhancement, while, for TM incidence, the actual matched-filter

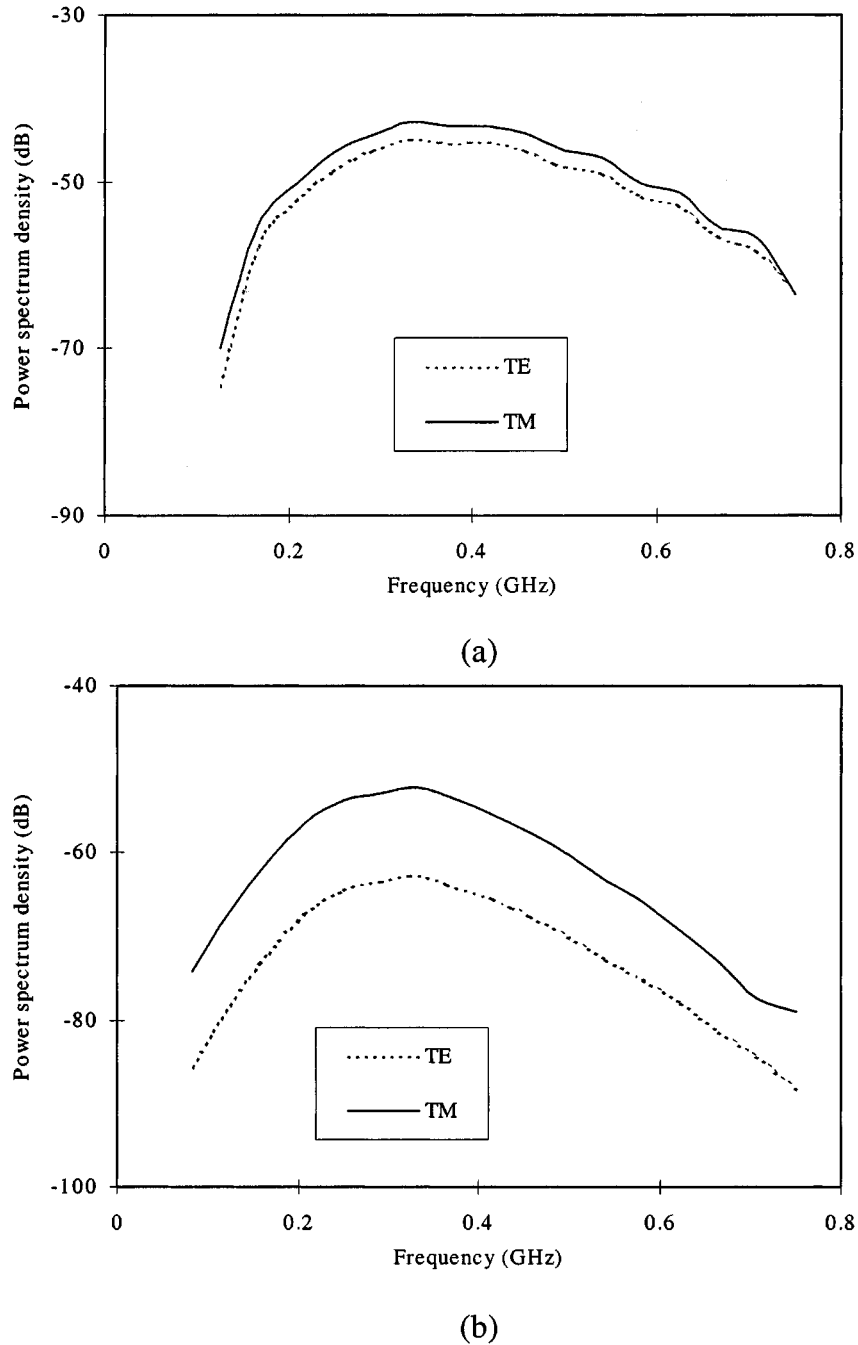


Fig. 5. Power spectral density for backscattered clutter induced by a Gaussian rough surface with mean height zero, variance 3.95 cm, and correlation length 18.75 cm, with results presented for TE and TM polarizations. (a) Incidence angle $\theta_i = 30^\circ$. (b) Incidence angle $\theta_i = 70^\circ$.

performance is close to those of the idealized results, and the optimal detector provides only a slight improvement. To explain this phenomenon, consider Fig. 10, in which we have plotted the relative power transmitted into the soil ($\epsilon_r = 6$ and $\sigma = 0.005\text{S/m}$) when the air-soil interface is flat, as a function of incidence angle, for both TE and TM polarization (i.e., we plot $1 - |\Gamma|^2$, where Γ is the flat-surface reflection coefficient). For incidence near $\theta_i = 70^\circ$, there is very little variation in $1 - |\Gamma|^2$ for TM polarization (due to the Brewster angle, and the corresponding stationary point in $1 - |\Gamma|^2$), while the variation for TE polarization is relatively strong. At the rough surface, the incident wave impinges the interface at angles that

vary randomly about θ_i . For the relatively modest roughness considered here, the random variation about θ_i is small. Therefore, from Fig. 10, one would expect that, for $\theta_i = 70^\circ$, the fields transmitted into the soil will be more randomized for TE polarization than for TM. Recall that the optimal detector is designed for problems in which the target signature is random, due to the stochastic nature of the fields transmitted through a random interface. Therefore, for $\theta_i = 70^\circ$ and relatively modest surface roughness, one would expect that a matched filter would be sufficient for TM polarization while the optimal detector would be most beneficial for TE excitation, consistent with the results in Figs. 8 and 9.

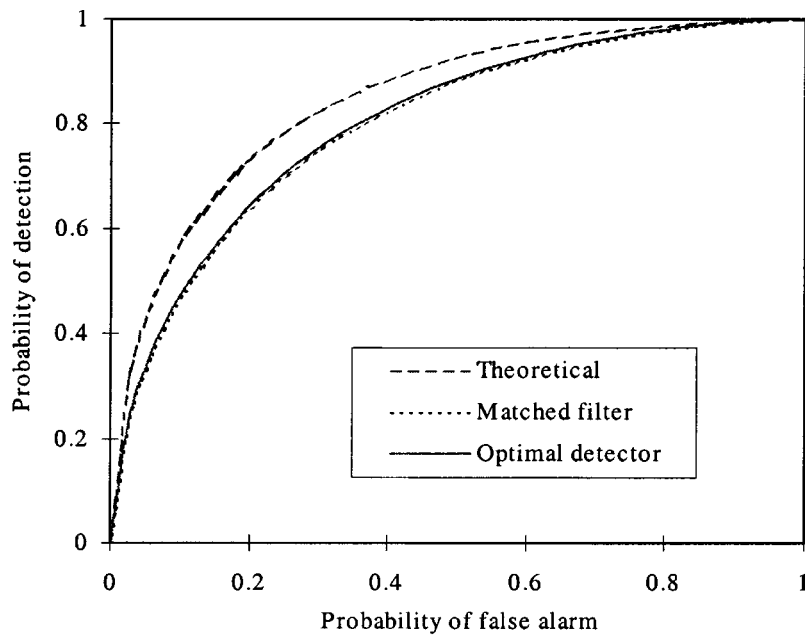


Fig. 6. Receiver operating characteristic for the target in Fig. 4 buried under the random rough surface in Fig. 5, for TE excitation at $\theta_i = 30^\circ$. Results are presented for idealized matched-filter performance (if the target signature were deterministic and known exactly), actual matched-filter performance, and for the optimal detector in Fig. 1.

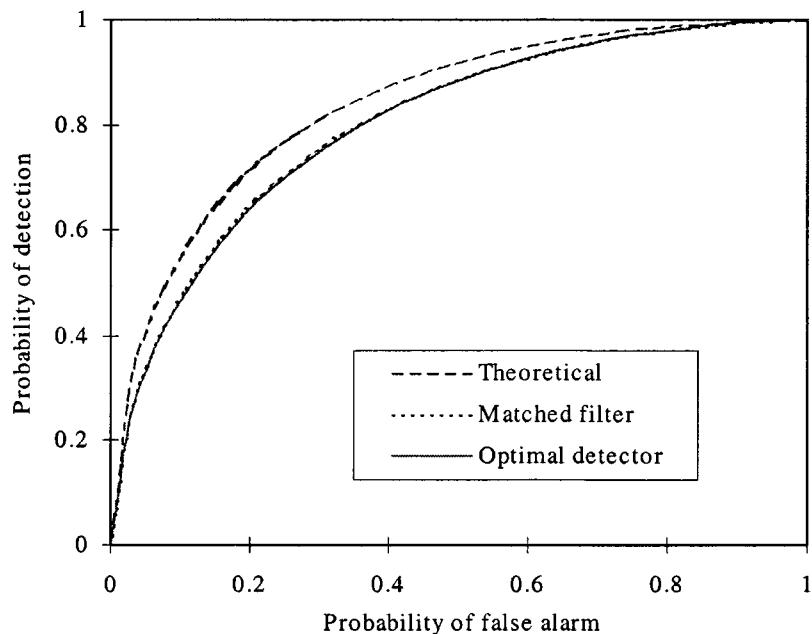


Fig. 7. As in Fig. 6, but for TM excitation.

With this insight, we return to the results for incidence angle $\theta_i = 30^\circ$. From Fig. 10, we see that the variation in $1 - |\Gamma|^2$ is relatively modest in the vicinity of $\theta_i = 30^\circ$, with similar variability seen for TE and TM excitation. Therefore, it is expected that the matched filter will do relatively well for such incidence angles (the transmitted fields only being weakly perturbed due to the random surface) and that modest improvements are expected from the optimal detector, consistent with Figs. 6 and 7.

Summarizing, if the variability of $\mathbf{s}(\theta_m)$ is large, the optimal detector will yield significant improvements relative to the matched filter. However, if the rough surface is such that the

fields which penetrate the interface are only weakly perturbed relative to the flat-surface response \mathbf{s} , the optimal detector reduces to a matched filter. To quantify such, we compute the mean and standard deviation of the correlation between $\mathbf{s}(\theta_m)$ and \mathbf{s} as

$$c_m = \frac{\mathbf{s}^T \mathbf{s}(\theta_m)}{\sqrt{\mathbf{s}^T \mathbf{s}} \sqrt{E[\mathbf{s}(\theta_m)^T \mathbf{s}(\theta_m)]}} \quad (5)$$

the results for which are tabulated in Table I for the examples in Figs. 6–9. From Table I, we see that the relative variation in $c, \sigma_c/m_c$, is small for TM polarization, at both $\theta_i = 30^\circ$ and

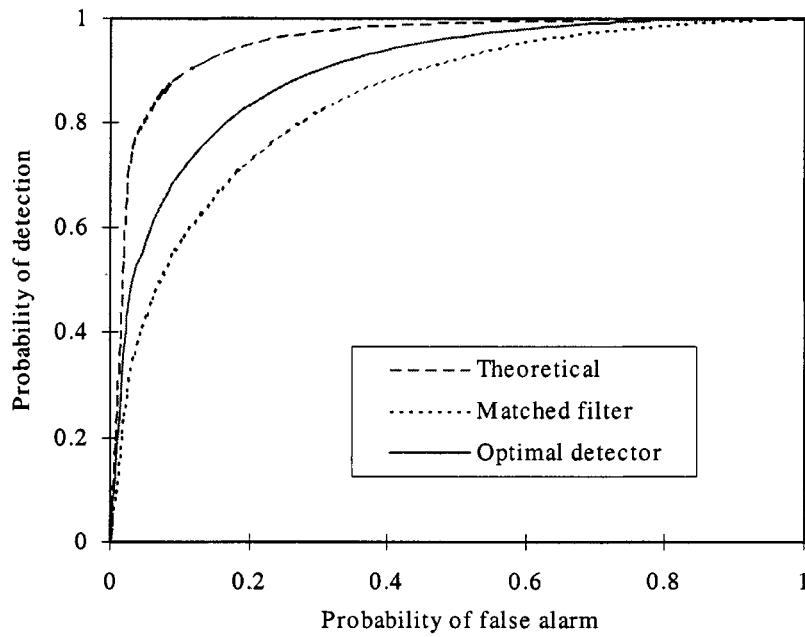


Fig. 8. Receiver operating characteristic for the target in Fig. 4 buried under the random rough surface in Fig. 5, for TE excitation at $\theta_i = 70^\circ$.

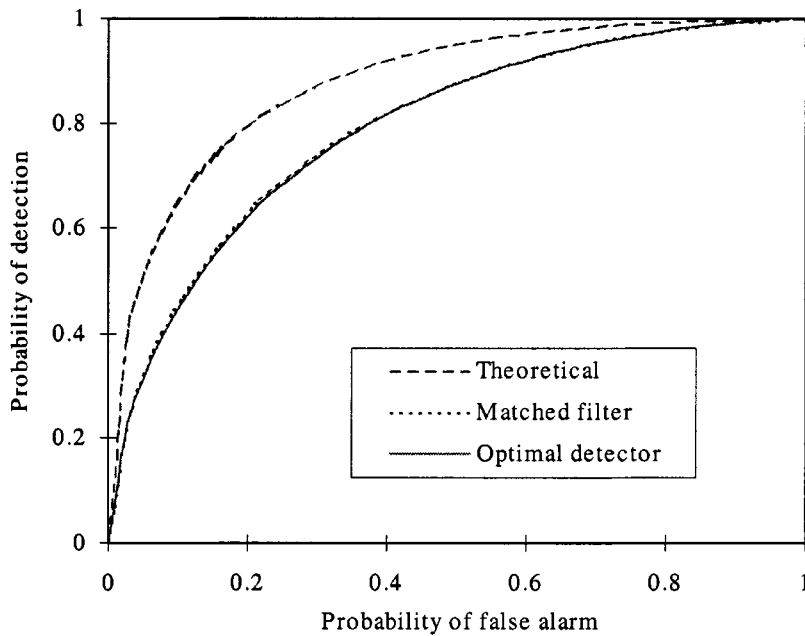


Fig. 9. As in Fig. 8, but for TM excitation.

TABLE I
MEAN AND STANDARD DEVIATION OF THE CORRELATION IN (5), FOR THE EXAMPLES IN FIGS. 6-9

	mean c , m_c	standard dev. of c , σ_c	σ_c/m_c
TE, $\theta_i=30^\circ$	0.6704	0.3703	0.5522
TM, $\theta_i=30^\circ$	0.7678	0.2943	0.3828
TE, $\theta_i=70^\circ$	0.5392	0.3970	0.7379
TM, $\theta_i=70^\circ$	0.6969	0.2593	0.3716

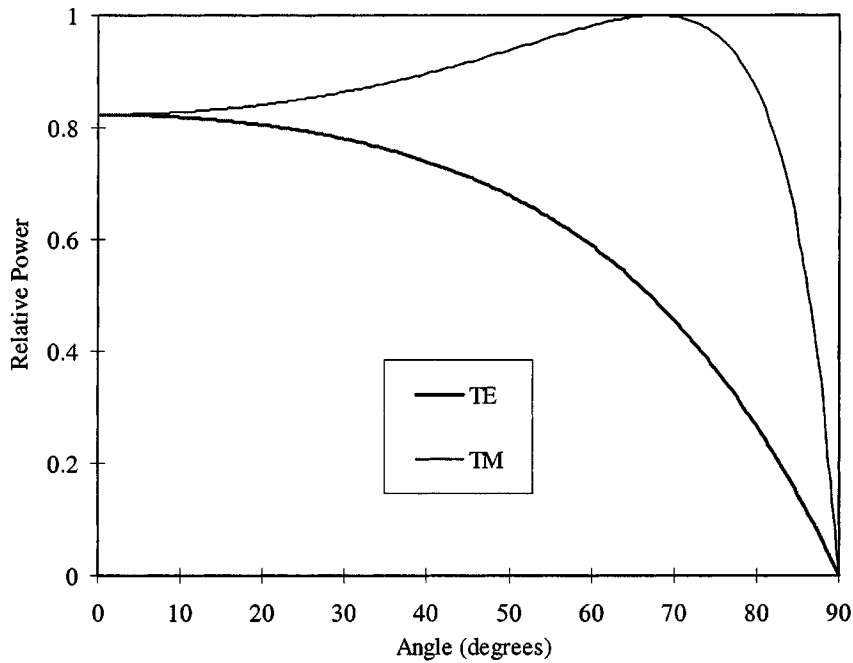


Fig. 10. Relative power transmitted into soil with $\epsilon_r = 6$ and $\sigma = 0.005$, as a function of incidence angle (flat air-ground interface).

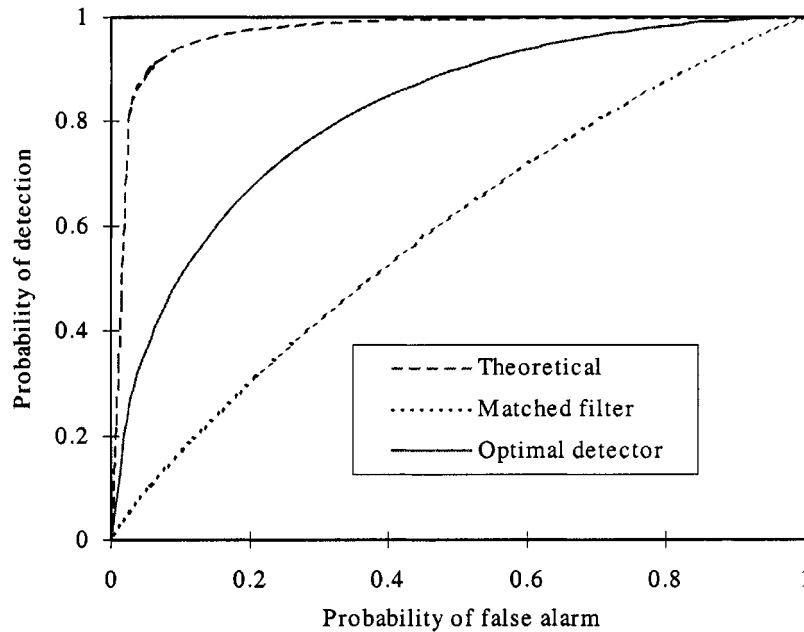


Fig. 11. Receiver operating characteristic as in Fig. 8 (TE polarization and $\theta_i = 70^\circ$), but considering a rough surface with variance 8.84 cm and correlation length 37.5 cm.

$\theta_i = 70^\circ$. The largest such variability occurs for TE excitation at $\theta_i = 70^\circ$, for which we saw the most dramatic performance gain manifested by the optimal detector.

D. Increased Surface Roughness

To demonstrate the effect of the optimal detector for a rougher surface, we consider the same soil and target as above, but now the Gaussian surface has a variance of 8.84 cm and a correlation length of 37.5 cm (we are allowing larger surface variance than before, but have also increased the correlation length, such that the surface is still relatively smoothly varying). We restrict

ourselves to $\theta_i = 70^\circ$, to examine if the increased surface variability produces enough randomness in the transmitted fields (and hence the target signature) such that the optimal detector yields gains, even for TM excitation. In Figs. 11 and 12 are plotted ROC curves for TE and TM polarization, respectively, in the same format as before. We see from these Figs. that the optimal detector yields significant performance improvement for TE excitation, as found in Fig. 8. Of more interest, in Fig. 12 we note that the increased level of surface variability has yielded optimal detector performance for TM polarization which is significantly superior to that of the matched filter. This underscores the

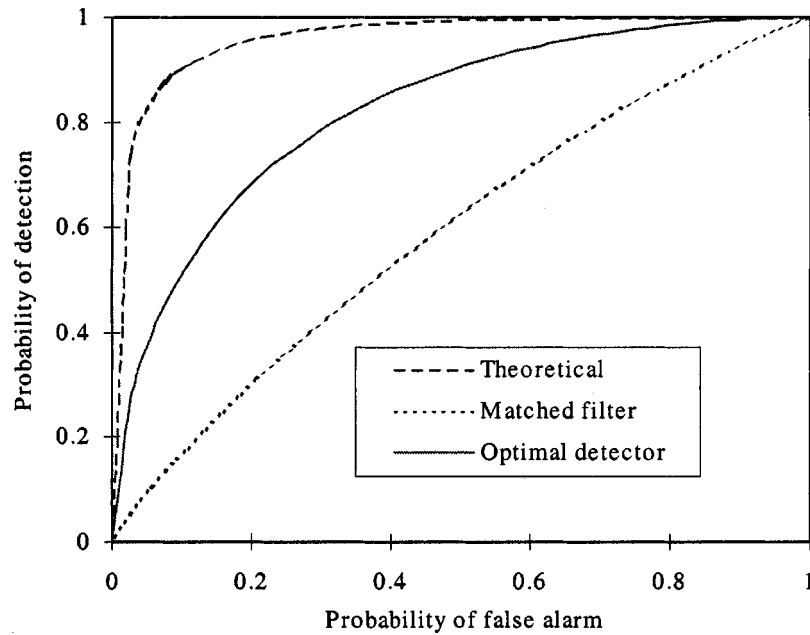


Fig. 12. As in Fig. 11, but for TM polarization.

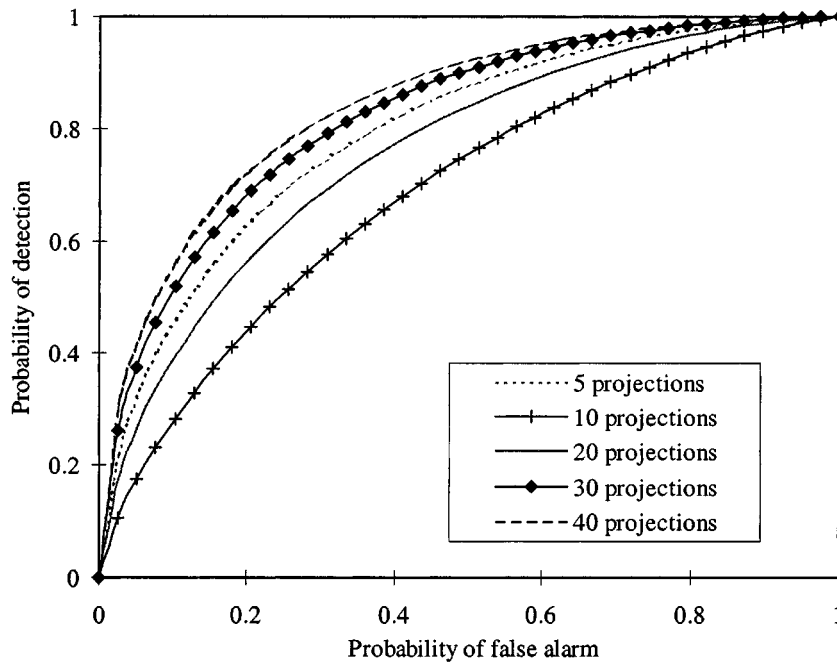


Fig. 13. Convergence of the optimal detector as a function of M [see (4)], for the example considered in Fig. 12.

fact that the performance gain accrued by the optimal detector is more significant as the transmitted fields (and, therefore, the target signature) becomes more random.

Because the surface is more random in these examples, one might expect the value of M required for convergence of the optimal detector will in turn be larger (relative to the results in Figs. 6–9). This was found to be the case; for the results in Figs. 11 and 12, we have found that M must be greater than about 40 to achieve convergence of (4). To examine the convergence of the optimal detector, in Fig. 13, we plot ROC curves as a function of M , considering TM excitation, $\theta_i = 70^\circ$, and the surface roughness in Figs. 11 and 12. For this relatively rough

surface, the optimal detector converges for $M > 40$ (recall from Fig. 8 that the less-rough surface only required $M > 20$). We note that one will generally not know *a priori* which value of M is required for a given problem, but the appropriate M can be determined adaptively by simply considering further projections $s(\theta_m)$ until convergence is achieved in (4).

E. General Observations

In the above examples, we have considered one soil type, one target, two angles of incidence, and two distributions for the rough-surface statistics. Therefore, it is difficult to draw general conclusions. However, we have demonstrated that, when

the surface roughness is sufficient to introduce randomization of the transmitted fields, the optimal detector yields improved performance relative to the matched filter. In many examples the performance enhancement was significant. To address the complexity of the optimal detector, note that it requires M projections onto waveforms $\mathbf{s}(\boldsymbol{\theta}_m)$ rather than a single projection onto the deterministic waveform \mathbf{s} , as per a matched filter. However, for a given target and surface roughness, the M waveforms $\mathbf{s}(\boldsymbol{\theta}_m)$ are computed once and stored, and can be used to test all \mathbf{e} characteristic of said target and clutter. For the problems considered here, M was a relatively small number (<50) and therefore the attendant significant performance gain in several cases appears to justify the associated modest escalation in complexity.

IV. CONCLUSION

An optimal detector has been presented for the time-domain detection of deterministic targets buried under a randomly rough air-ground interface. The random character of the fields scattered from and penetrating through the random interface requires the parametrization of the clutter and buried-target signature as random processes, generally with different statistics. For the Gaussian surfaces considered here, we have found the clutter characterized as a correlated (nonwhite) Gaussian random process. Therefore, the optimal detector invokes a whitening filter. While in principle the optimal detector requires the statistics of the target signature, such are not easily quantified in general. Therefore, we have implemented the optimal detector approximately via Monte Carlo integration, utilizing M realizations of the random target signature, generated from M realizations of the rough surface.

For the examples considered here, designed to be of interest for buried-target detection, we have found that M should be greater than approximately forty to achieve convergence. However, this number is a function of the degree of randomness in the target signature and was found to increase as the surface became more rough. The enhancement in detector performance yielded by the optimal detector depends as well on the degree to which the target is stochastic. Interestingly, we found that for relatively modest roughness the signature was minimally randomized for vertical polarization near the Brewster angle, at which the transmitted power has a stationary point as a function of incidence angle. However, this phenomenon was vitiated when the roughness became more severe, and the optimal detector then provided dramatic improvements in detector performance.

In the examples considered here, the soil properties, target depth, and target orientation were assumed known, and all randomness was induced by the rough surface. In practice, these parameters will not be known and must be treated statistically. For example, for the detection of buried mines or unexploded ordnance, the target depth will be unknown, but there is likely to be *a priori* knowledge as to its statistical distribution, with similar issues holding for the soil properties and target orientation. Therefore, in the context of the optimal detector in (4), one must perform Monte Carlo integration over these parameters as well. With the large number of random parameters that one may encounter in practice, and the need to consider a sufficient number of waveforms M to span the statistical space of same, it is essen-

tial that the forward algorithm used to compute each waveform (from a statistical ensemble) be as fast as possible. This will be an area of future research, constituting the synergy of fast forward algorithms and target detection for random scattering, much as fast forward algorithms have played a critical role in the development of inverse-scattering algorithms for deterministic scattering.

REFERENCES

- [1] M. Saillard and D. Maestre, "Scattering from metallic and dielectric rough surfaces," *J. Opt. Soc. Amer. A.*, vol. 7, pp. 982–990, June 1990.
- [2] —, "Scattering from random rough surfaces: A beam simulation method," *J. Opt.*, vol. 19, pp. 173–176, 1988.
- [3] E. Bahar and Y. Zhang, "A new unified full-wave approach to evaluate the scatter cross sections of composite random rough surfaces," *IEEE Trans. Geosci. Remote Sens.*, vol. 34, pp. 973–980, July 1996.
- [4] A. Nashahibi, F. T. Ulaby, and K. Sarabandi, "Measurement and modeling of the millimeter-wave backscatter response of soil surface," *IEEE Trans. Geosci. Remote Sens.*, vol. 34, pp. 561–572, Mar. 1996.
- [5] R. M. Narayanan, R. Pardipuram, and D. C. Rudquist, "Statistical characteristics of simulated radar imagery from bare soil surfaces: Effects of surface roughness and soil moisture variability," *IEEE Trans. Geosci. Remote Sens.*, vol. 32, pp. 159–168, Jan. 1994.
- [6] A. Ishimaru, *Wave Propagation and Scattering in Random Media*. New York: Academic, 1978.
- [7] F. D. Hastings, J. B. Schneider, and S. L. Broschat, "A Monte-Carlo FDTD technique for rough surface scattering," *IEEE Trans. Antennas Propagat.*, vol. 43, pp. 1183–1191, Nov. 1995.
- [8] G. S. Brown, "A new approach to the analysis of rough surface scattering," *IEEE Trans. Antennas Propagat.*, vol. 39, pp. 943–948, July 1991.
- [9] T. Dogaru and L. Carin, "Time-domain sensing of a target buried under a rough air-ground interface," *IEEE Trans. Antennas Propagat.*, vol. 46, pp. 360–372, Mar. 1998.
- [10] H. L. Van Trees, *Detection, Estimation, and Modulation Theory*. New York: Wiley, 1968.
- [11] A. Papoulis, *Probability, Random Variables, and Stochastic Processes*, 2nd ed. New York: McGraw-Hill, 1984.
- [12] M. Moghaddam and W. C. Chew, "Study of some practical issues in inversion with the Born iterative method using time-domain data," *IEEE Trans. Antennas Propagat.*, vol. 41, pp. 177–184, Feb. 1993.
- [13] C.-C. Chiu and Y.-W. Kiang, "Electromagnetic inverse scattering of a conducting cylinder buried in a lossy half-space," *IEEE Trans. Antennas Propagat.*, vol. 40, pp. 1562–1565, Aug. 1992.
- [14] K. S. Yee, "Numerical solution of initial boundary value problems involving Maxwell's equations in isotropic media," *IEEE Trans. Antennas Propagat.*, vol. AP-14, pp. 302–307, 1966.
- [15] K. S. Kunz and R. J. Luebbers, *The Finite Difference Time Domain Method for Electromagnetics*. Boca Raton, FL: CRC Press, 1993.
- [16] A. Taflov, *Computational Electrodynamics: The Finite-Difference Time-Domain Method*. Norwood, MA: Artech, 1995.
- [17] P. G. Petropoulos, "Stability and phase error analysis of FDTD in dispersive dielectrics," *IEEE Trans. Antennas Propagat.*, vol. 42, pp. 62–69, Jan. 1994.
- [18] —, "Phase error control for FDTD methods of second and fourth order accuracy," *IEEE Trans. Antennas Propagat.*, vol. 42, pp. 859–862, June 1994.
- [19] D. E. Merewether, R. Fisher, and F. W. Smith, "On implementing a numerical Huygens surface in a finite difference program to illuminate scattering bodies," *IEEE Trans. Nuclear Sci.*, vol. NS-27, pp. 1829–1833, Dec. 1980.
- [20] T.-T. Hsu and L. Carin, "FDTD analysis of plane-wave diffraction from microwave devices on an infinite dielectric slab," *IEEE Microwave Guided Wave Lett.*, vol. 6, pp. 16–18, Jan. 1996.
- [21] G. Mur, "Absorbing boundary conditions for the finite-difference approximation of the time-domain electromagnetic-field equations," *IEEE Trans. Electromagn. Compat.*, vol. EMC-23, pp. 377–382, Nov. 1981.
- [22] R. L. Higdon, "Absorbing boundary conditions for difference approximations to the multi-dimensional wave equations," *Math. Comput.*, vol. 47, no. 176, pp. 437–459, Oct. 1986.
- [23] J. P. Berenger, "A perfectly matched layer for the absorption of electromagnetic waves," *J. Comput. Phys.*, vol. 114, pp. 185–200, Oct. 1994.

- [24] D. Katz, E. Thiele, and A. Taflove, "Validation and extension to three dimensions of the Berenger PML absorbing boundary condition for FD-TD meshes," *IEEE Microwave Guided Wave Lett.*, vol. 4, pp. 268–270, Aug. 1994.
- [25] W. C. Chew and W. Weedon, "A 3D perfectly matched medium from modified Maxwell's equations with stretched coordinates," *Microwave Opt. Technol. Lett.*, vol. 7, pp. 599–604, Sept. 1994.
- [26] J. Fang and Z. Wu, "Generalized perfectly matched layer—An extension of Berenger's perfectly matched layer boundary condition," *IEEE Microwave Guided Wave Lett.*, vol. 5, pp. 451–453, Dec. 1995.
- [27] Z. Wu and J. Fang, "Numerical implementation and performance of perfectly matched layer boundary condition for waveguide structures," *IEEE Trans. Microwave Theory Tech.*, vol. 43, pp. 2676–2683, Dec. 1995.
- [28] K. Umashankar and A. Taflove, "A novel method to analyze electromagnetic scattering of complex objects," *IEEE Trans. Electromagn. Compat.*, vol. EMC-24, pp. 397–405, Nov. 1982.
- [29] A. Taflove and K. Umashankar, "Radar cross section of general three-dimensional scatterers," *IEEE Trans. Electromagn. Compat.*, vol. EMC-25, pp. 433–441, Nov. 1983.
- [30] K. Demarest, Z. Huang, and R. Plumb, "An FDTD near-to-far-zone transformation for scatterers buried in stratified grounds," *IEEE Trans. Antennas Propagat.*, vol. 44, pp. 1150–1157, Aug. 1996.
- [31] S. Haykin, *Adaptive Filter Theory*, 3rd ed. Upper Saddle River, NJ: Prentice-Hall, 1996.
- [32] P. Hubral and M. Tygel, "Analysis of the Rayleigh pulse," *Geophys.*, vol. 54, pp. 654–658, 1989.
- [33] M. A. Ressler and J. W. McCorkle, "Evolution of the Army Research Laboratory ultra-wideband test bed," in *Ultra-Wideband Short-Pulse Electromagnetics 2*, L. Carin and L. B. Felsen, Eds. New York: Plenum Press, 1995, pp. 109–123.
- [34] S. Vitebskiy, L. Carin, M. Ressler, and F. Le, "Ultra-wideband, short-pulse ground-penetrating radar: Theory and measurement," *IEEE Trans. Geosci. Remote Sens.*, vol. 35, pp. 762–772, May 1997.
- [35] J. E. Hipp, "Soil electromagnetic parameters as functions of frequency, soil density, and soil moisture," *Proc. IEEE*, vol. 62, pp. 98–103, Jan. 1974.



Traian Dogaru was born in Bucharest, Romania, in 1966. He received the engineering degree from the Polytechnic University of Bucharest in 1990. He received the M.S. degree in electrical engineering and the Ph.D. degree from Duke University, Durham, NC, in 1997 and 1999, respectively.

From 1992 to 1995, he held different engineering positions in the magnetic recording industry. Currently, he is a Research Associate with Duke University. His research interests are in electromagnetic wave theory, computational electromagnetics, rough surface scattering and radar-related signal processing.

Leslie Collins (M'96) was born in 1963 in Raleigh, NC. She received the B.S.E.E. degree from the University of Kentucky, Lexington, the M.S.E.E. and the Ph.D. degree both in electrical engineering, from the University of Michigan, Ann Arbor, in 1985, 1986 and 1995, respectively.

From 1986 to 1990, she was a Senior Engineer with the Westinghouse Research and Development Center, Pittsburgh, PA. In 1995, she joined the Electrical and Computer Engineering Department at Duke University, Durham, NC., as an Assistant Professor. Her current research interests include incorporating physics-based models into statistical signal processing algorithms and she is pursuing applications in subsurface sensing as well as enhancing speech understanding by hearing impaired individuals.

Dr. Collins is a member of Tau Beta Pi, Eta Kappa Nu, and Sigma Xi honor societies.

Lawrence Carin (S'86–M'89–SM'96) was born in Washington, DC., on March 25, 1963. He received the B.S., M.S., and Ph.D. degrees in electrical engineering, from the University of Maryland, College Park, in 1985, 1986, and 1989, respectively.

In 1989, he joined the Electrical Engineering Department at Polytechnic University, Brooklyn, NY., as an Assistant Professor, and in 1994, became an Associate Professor. In 1995, he joined the Electrical Engineering Department at Duke University, Durham, NC., where he is an Associate Professor. Currently, he is principal investigator on a Multidisciplinary University Research Initiative (MURI) on demining. He is an Associate Editor of the IEEE TRANSACTIONS ON ANTENNAS AND PROPAGATION. His current research interests include short-pulse scattering, subsurface sensing, and wave-based signal processing.

Dr. Carin is a member of the Tau Beta Pi and Eta Kappa Nu honor societies.